Leaching surfaces to characterize transport in a heterogeneous aquifer: Comparison between flux concentrations, resident concentrations, and flux concentrations estimated from temporal moment analysis

E. Bloem,[1,2] J. Vanderborght,[3] and G. H. de Rooij[1]

[1]   For subsurface solute transport, flux concentrations are key, while usually resident concentrations are measured. Flux concentrations are frequently estimated from resident concentrations by temporal moment analysis. We tested this approach by simulating transport of an injected tracer during steady flow in an aquifer with a heterogeneous saturated hydraulic conductivity. We constructed grid cell–scale breakthrough curves (BTCs) from flux concentrations and approximated BTCs from resident concentrations and estimated flux concentrations. We assembled these BTCs into spatiotemporal leaching surfaces at various aquifer cross sections for subsequent analysis. Resident concentrations were unsuitable to assess solute movement in the aquifer. Temporal moment analysis worked well when the entire aquifer cross section was considered but performed poorer at the grid cell scale because it approximates the local velocity by the trajectory average. The leaching surfaces served as valuable tools to demonstrate and quantify the limitations of temporal moment analysis.

Citation: Bloem, E., J. Vanderborght, and G. H. de Rooij (2008), Leaching surfaces to characterize transport in a heterogeneous aquifer: Comparison between flux concentrations, resident concentrations, and flux concentrations estimated from temporal moment analysis, *Water Resour. Res.*, *44*, W10412, doi:10.1029/2007WR006425.

1.   Introduction

[2]   Fresh groundwater is an important source of potable water. In order to preserve this valuable resource for future generations, it needs to be protected against contamination by point and diffuse pollution sources, and contaminated aquifers need to be cleaned up. Natural aquifer heterogeneity influences the transport and fate of contaminants [*Anderson*, 1987] and thus profoundly affects groundwater remediation projects, the effectiveness of natural attenuation, and risk assessments of a given contaminant plume contaminating drinking water wells or surface water. To improve treatment strategies, the predictability of natural attenuation, and risk assessments, we require a better understanding of the effect of heterogeneity on contaminant movement in aquifers.

[3]   Experiments involving the injection of solutes into an aquifer are difficult and can usually only be performed under legal restrictions. Consequently, experimental programs have been executed at a limited number of aquifers (the Borden aquifer [*Sudicky et al.*, 1983; *Mackay et al.*, 1986; *Freyberg*, 1986; *Sudicky*, 1986], Twin Lake site [*Killey and*

Moltyaner, 1988; *Moltyaner and Killey*, 1988; *Dagan et al.*, 1997], Cape Cod field [*LeBlanc et al.*, 1991; *Garabedian et al.*, 1991; *Hess et al.*, 1992; *Rubin and Ezzedine*, 1997; *Woodbury and Rubin*, 2000], Columbus [*Boggs et al.*, 1992; *Adams and Gelhar*, 1992; *Rehfeldt et al.*, 1992], Horkheimer Insel [*Ptak and Teutsch*, 1994; *Ptak and Schmid*, 1996], and the Krauthausen site [*Vereecken et al.*, 2000; *Vanderborght and Vereecken*, 2001]). In order to investigate mixing and the spatial variability of the advection and mixing processes, in most tracer tests, local concentrations are measured using local groundwater samplers or multilevel samplers, which only minimally disturb the flow field.

[4]   Spatial or temporal moment analysis of resident concentration [*Parker and van Genuchten*, 1984] measurements in a tracer field experiment is often used to obtain parameters characterizing flow and transport in heterogeneous aquifers. Description of solute transport in terms of the positions of solute particles or the spatial distribution of solute concentrations at fixed times targets the spatial moments of a solute plume [*Aris*, 1956; *Freyberg*, 1986; *Garabedian et al.*, 1991; *Adams and Gelhar*, 1992; *Vereecken et al.*, 2000]. Transport of solutes described in terms of the arrival times of solutes or temporal evolution of solute fluxes at fixed monitoring planes considers the temporal moments of solute breakthrough curves (BTCs) [*Kreft and Zuber*, 1978; *Ptak and Schmid*, 1996; *Dagan et al.*, 1997; *Rubin and Ezzedine*, 1997; *Vanderborght and Vereecken*, 2001].

[5]   Temporal moment analysis is considered more efficient than spatial moment analysis [*Rubin and Ezzedine*,

[1]Soil Physics, Ecohydrology and Groundwater Management, Environmental Sciences Group, Wageningen University, Wageningen, Netherlands.
[2]Now at Bioforsk, Norwegian Institute for Agricultural and Environmental Research, Ås, Norway.
[3]Agrosphere, ICG-4, Forschungszentrum Jülich, Jülich, Germany.

1997], because accurate estimates of spatial moments require a large number of samplers, distributed over a large area with a sufficiently high spatial resolution. Installing that many wells may not be allowed at some sites and will often be prohibitively expensive. The development of techniques to continuously monitor radioactive [*Killey and Moltyaner*, 1988; *Moltyaner and Killey*, 1988] or fluorescent [*Ptak and Teutsch*, 1994; *Ptak and Schmid*, 1996] tracer concentrations also stimulates the characterization of transport in aquifers using temporal moments [*Vanderborght and Vereecken*, 2001].

[6] As illustrated in the experiments mentioned above, solute monitoring in the field is usually limited to observations of resident concentrations, whereas solute fluxes are relevant quantities for estimating solute travel times [e.g., *Dagan et al.*, 1992]. Flux concentrations across a monitoring plane should be measured by collecting all the water flowing across the monitoring plane and measuring the concentration in the collected water. This strategy strongly reduces the spatial resolution and results in a massive disturbance of the flow field. More realistically, a limited number of pumping wells downstream from the injection can capture a portion of the water flowing through the monitoring plane. Using this approach, integrated measures of the transport process are obtained. The disturbance of the flow field by pumping, and mixing occurring close to and within the pumping well, change the tracer breakthrough as compared to the natural flow conditions, which makes the interpretation of the measured tracer breakthrough more difficult.

[7] Theoretically, the passage of a solute across the monitoring plane could be calculated from locally measured concentrations if it is assumed that the locally measured concentrations represent local flux concentrations and that local water fluxes are available. The first assumption is only valid if local concentration variations are sufficiently small. The latter criterion is also problematic since local water flow measurements are extremely difficult. *Vanderborght and Vereecken* [2001] discussed ways to approximate flux concentrations in a monitoring plane on the basis of local resident concentration measurements. In one approach, they proposed to approximate the local water flux from the advection velocity of the tracer toward the observation point, which was derived from temporal moments of the locally measured time series of resident concentrations. To assess the merit of using resident concentrations to estimate solute fluxes, numerical simulations are at this time a more powerful tool than direct measurements. On the basis of numerical simulations of transport in a generated heterogeneous aquifer, *Vanderborght et al.* [2005] demonstrated that advection velocities estimated from local resident concentrations in time could be used as proxies for local water fluxes to calculate average solute fluxes across a reference surface.

[8] One way of characterizing the heterogeneity of the transport process is to determine the variability and spatial correlation of locally observed peak arrival times. Since the peak concentration arrival time and the mean particle arrival time derived from a locally measured BTC are predominantly determined by the advection velocity of the tracer toward the observation point, the variability of peak or mean arrival times at several locations contains valuable information about the heterogeneity of the aquifer. Information about the spatial variability of peak or mean arrival

times was used by, e.g., *Rubin and Ezzedine* [1997], *Woodbury and Rubin* [2000], *Vanderborght and Vereecken* [2001], *Bellin and Rubin* [2004], and *Vanderborght et al.* [2005] to infer geostatistical parameters that characterize the aquifer heterogeneity. As an alternative measure to characterize transport heterogeneity, *de Rooij and Stagnitti* [2002a, 2002b, 2004] recently presented the leaching surface as a tool to analyze the spatially and temporally nonuniform passage of solutes across a monitoring plane. The leaching surface is a curved surface constructed from a population of local-scale BTCs, thus preserving all information present in these BTCs. At present, the method has only been applied to unsaturated, macroscopically vertical solute transport in soils. For saturated, macroscopically unidirectional flows, the leaching surface method can be readily applied if a solute pulse is applied uniformly across a cross section of the flow domain perpendicular to the macroscopic flow direction. The downstream monitoring plane(s) must be perpendicular to the main flow.

[9] The objective of this paper is to characterize the effect of second-order stationary heterogeneity of the saturated hydraulic conductivity in an aquifer on solute transport in a flow field undisturbed by groundwater extractions (which otherwise would cause additional solute redistribution). In order to do so, we apply the leaching surface methodology to a groundwater flow problem for the first time.

[10] It is well established that flux concentrations should be used for quantifying solute movement, but these are often not available. Consequently, modelers and practitioners have to rely on resident concentrations. This introduces an unavoidable error, that can as yet not be quantified. A second objective is therefore to assess the validity of resident concentrations for quantifying solute migration. Leaching surfaces at various distances from the solute application plane were constructed for both resident concentrations and flux concentrations allowing investigation of their interchangeability. We also evaluated the potential of temporal moment analysis in solute movement problems by determining the first moments of local-scale time series of resident concentrations in order to derive flux concentrations from local resident concentrations. We constructed approximate leaching surfaces from those and compared these with the correct leaching surfaces.

2. Materials and Methods

2.1. Aquifer

[11] A steady state saturated water flow in the 3D domain $0 \leq x_1 \leq 100$ m, $0 \leq x_2 \leq 100$ m, $0 \leq x_3 \leq 20$ m (x_1, x_2: horizontal coordinates [L], x_3: vertical coordinate [L]) was simulated using the finite element code TRACE [*Vereecken et al.*, 1994]. The size of the grid blocks was 0.5 m in the horizontal directions (x_1 and x_2) and 0.1 m in the vertical direction (x_3). At the bottom and top boundaries ($x_3 = 0$ and $x_3 = L_3 = 20$ m) and at the two lateral boundaries ($x_1 = 0$ and $x_1 = L_1 = 100$ m), a zero flow or zero hydraulic head gradient boundary condition was implemented. At the front and back surfaces ($x_2 = 0$ and $x_2 = L_2 = 100$ m), a constant hydraulic head distribution was defined so that the general mean hydraulic head gradient $\langle \nabla \psi(\mathbf{x}) \rangle = (0, -10^{-3}, 0)^T$ where ψ [L] denotes the hydraulic head, $\mathbf{x}$ [L] is the coordinate vector, superscript T denotes the transpose of the superscripted matrix, and $\langle a(\mathbf{x}) \rangle$ is the arithmetic mean

of function a over the flow domain. The porosity n [−] was uniform at 0.25, while g [−] (the log-transformed scaled hydraulic conductivity)

$$g(\mathbf{x}) = \ln\left[\frac{K(\mathbf{x})}{K_0}\right] \qquad (1)$$

had zero mean and unit variance. The geometric mean K_0 [L T^{-1}] of the hydraulic conductivity K [L T^{-1}] was set to 250 m d^{-1}, resulting in a mean pore water velocity $\langle \mathbf{v}(\mathbf{x}) \rangle$ of 1 m d^{-1} in the direction of x_2, where $\mathbf{v}$ [L T^{-1}] is the pore water velocity vector. The random field $g(\mathbf{x})$ was second-order stationary with an exponential covariance structure

$$E[g(\mathbf{x})g(\mathbf{x}+\mathbf{h})] = \sigma_g^2 \exp\left[-\sqrt{\frac{h_1^2}{\gamma_1^2} + \frac{h_2^2}{\gamma_2^2} + \frac{h_3^2}{\gamma_3^2}}\right] \qquad (2)$$

where $\mathbf{h}$ [L] denotes the separation vector with elements h_i [L] (with $i \in 1, 2, 3$ indicating the direction), γ_i [L] is the correlation length in direction i, and σ_g^2 is the variance of $g(\mathbf{x})$. In this model $\gamma_1 = \gamma_2 = 5$ m and $\gamma_3 = 1$ m. One realization of the heterogeneous field was generated using a Kraichnan generator [Kraichnan, 1970].

2.2. Numerical Tracer Experiment

[12] Solute transport was described by the convection-dispersion equation

$$\frac{\partial C^r(\mathbf{x},t)}{\partial t} = -\nabla[\mathbf{v}(\mathbf{x})C^r(\mathbf{x},t)] + \nabla \cdot [\mathbf{D}(\mathbf{x})\nabla C^r(\mathbf{x},t)] \qquad (3)$$

where t [T] denotes time, C^r is the solute resident concentration [M L^{-3}], and the elements D_{ij} [L^2 T^{-1}] of the dispersion tensor $\mathbf{D}$ [L^2 T^{-1}] are given, neglecting molecular diffusion, by Bear [1972]

$$D_{ij}(\mathbf{x}) = \lambda_T |\mathbf{v}| \delta_{ij} + (\lambda_L - \lambda_T)\frac{v_i v_j}{|\mathbf{v}|} \qquad (4)$$

where i and j denote coordinate directions, λ_L [L] and λ_T [L] denote the lateral and transversal dispersivity, respectively, and δ_{ij} is the Kronecker delta. In this study, $\lambda_L = 0.1$ m and $\lambda_T = 0.01$ m. Vanderborght et al. [2005, Figure 9] found macrodispersivities of about 4 m in this aquifer, which is consistent with field observations of aquifers with comparable dimensions reviewed by Gelhar et al. [1992, Figures 2 and 3].

[13] For the transport simulations, the particle tracking code PARTRACE [Neuendorf, 1997] was used. A uniform initial tracer concentration C_0 at time $t = 0$ was assumed of 0.5 m thickness in the x_2 direction at $x_2 = 20$ m in the region 25 m $< x_1 < 75$ m and 5 m $< x_3 < 15$ m. Outside the injection slab, the flow domain was initially solute free. In total, 10^8

particles were injected at $t = 0$ in the injection slab and their displacement in the flow field was tracked. In the terminology proposed by Jury and Scotter [1994] this represents an initial value problem. The solute mass in each stream tube is proportional to its water content at the solute application plane (10^4 particles per grid block, $C_0 = 4 \times 10^5$ particles m^{-3}). Local-scale dispersion was modeled by adding a random displacement $Z\mathbf{B}\sqrt{\Delta t}$ to the advective displacement, where Δt is the time step, Z is a random variable drawn from Gaussian distribution with mean 0 and variance 1, and $\mathbf{B}$ a matrix that is related to the local-scale dispersion tensor as: $\mathbf{B} \cdot \mathbf{B}^T = \mathbf{D}$. Expansion of the final term of equation (3) leads to a term involving the gradient of $\mathbf{D}(\mathbf{x})$, which, according to equation (4), depends on the velocity field $\mathbf{v}$. We assumed that the aquifer heterogeneity was such that the local variation in $\mathbf{v}$ was small enough to make the term involving the gradient of $\mathbf{D}$ negligible. Concentration distributions were calculated until 150 days after tracer injection at daily intervals by counting the number of particles in the volumetric grid elements. The passage of the tracer was monitored at vertical monitoring planes downstream in the direction of increasing x_2 at $\Delta x_2 = 10, 30, 50,$ and 70 m from the tracer injection plane, with 25 m $< x_1 < 75$ m and 5 m $< x_3 < 15$ m. Thus, the size of the monitoring planes equaled that of the solute injection plane. This helped to avoid having substantial areas in the domain without any solutes, which would have hampered the solute transport analysis.

2.3. Tracer Plume Analysis
2.3.1. Resident and Flux Concentrations and Masses

[14] We analyzed the properties of the tracer plume as it passed the monitoring planes, and the evolution of these properties as the travel distance increased. To do so, we calculated resident solute concentrations, and flow velocity components v_2 perpendicular to the monitoring planes, for all cubes for which the four downstream corner nodes were located in one of the monitoring planes. The values of v_2 were obtained from the average of the eight corner nodes, and the resident concentrations resulted from the number of particles in the cubes. For a solute plume passing a monitoring plane, the flux concentration is a more relevant parameter than the resident concentration [Parker and van Genuchten, 1984; Jury and Roth, 1990]. The flux concentration C^f is defined as [Jury and Roth, 1990]

$$C^f(\mathbf{x},t) = \frac{J_s(\mathbf{x},t)}{J_w(\mathbf{x})} \qquad (5)$$

where $J_s(\mathbf{x}, t)$ [ML^{-2} T^{-1}] the solute flux in the main flow direction and $J_w(\mathbf{x})$ [L T^{-1}] the water flux in the main flow direction.

[15] A more formal definition is

$$C^f(x_1,x_3,t,x_2) = \lim_{\Delta x_1^* \downarrow 0 \Delta x_3^* \downarrow 0 \Delta t \downarrow 0} \frac{\displaystyle\int_{x_1-\frac{1}{2}\Delta x_1^*}^{x_1+\frac{1}{2}\Delta x_1^*} \int_{x_3-\frac{1}{2}\Delta x_3^*}^{x_3+\frac{1}{2}\Delta x_3^*} \int_{t-\frac{1}{2}\Delta t}^{t+\frac{1}{2}\Delta t} q_2(\xi_1,\xi_3,\chi,x_2)C(\xi_1,\xi_3,\chi,x_2)\mathrm{d}\chi\mathrm{d}\xi_3\mathrm{d}\xi_1}{\displaystyle\int_{x_1-\frac{1}{2}\Delta x_1^*}^{x_1+\frac{1}{2}\Delta x_1^*} \int_{x_3-\frac{1}{2}\Delta x_3^*}^{x_3+\frac{1}{2}\Delta x_3^*} \int_{t-\frac{1}{2}\Delta t}^{t+\frac{1}{2}\Delta t} q_2(\xi_1,\xi_3,\chi,x_2)\mathrm{d}\chi\mathrm{d}\xi_3\mathrm{d}\xi_1} \qquad (6)$$

The derivation of this equation is presented in Appendix A. Because the concentration and flow velocity within a cube and within a time interval are necessarily uniform in our numerical model, the resident and flux concentrations are equal at this smallest scale (see Appendix A) if the dispersive and diffusive fluxes are small compared to the advective solute flux. In our aquifer the Peclet number ($\Delta x_2/\lambda_L$, with Δx_2 the lateral travel distance [Bolt, 1982]) ≥ 100 for all monitoring planes, so in areas with appreciable solute transport this will generally be the case; in low-flow areas this assumption may be invalid, but these regions only marginally affect solute movement. The mass that resides in a cube at a given time or the mass flux through its walls (neglecting molecular diffusion) during a time interval will generally be different

$$M_{p,b}^r = n \cdot \Delta x_1^* \cdot \Delta x_2^* \cdot \Delta x_3^* \cdot C_{p,b}^r \tag{7}$$

$$M_{p,b}^f = n \cdot v_{2,p,b} \cdot \Delta x_1^* \cdot \Delta x_3^* \cdot \Delta t_b \cdot C_{p,b}^r \tag{8}$$

where $M_{p,b}^r$ [M] is the mass residing in cube p with $\Delta x_1^* = 0.5$ m, $\Delta x_2^* = 0.5$ m, and $\Delta x_3^* = 0.1$ m, at the end of the bth time interval ($\triangle t_b$ [T]). The superscript $*$ serves to distinguish the grid-scale length intervals from the larger-scale travel distances elsewhere in the paper. $M_{p,b}^f$ [M] is the mass convectively moving in the x_2 direction through the downstream wall of cube p during $\triangle t_b$. Since the porosity n is uniform, weighting according to water content was not necessary. From equations (7) and (8) we have

$$\frac{M_{p,b}^f}{M_{p,b}^r} = \frac{v_{2,p,b} \cdot \Delta t_b}{\Delta x_2^*} \tag{9}$$

At scales larger than that of individual cells, the variation of the flow field complicates the relationship between M^f and M^r. As a consequence, the resident and flux concentrations defined for volumes and planes larger than that of individual cells will no longer be identical.

2.3.2. Temporal Moment Analysis

[16] In practice, resident rather than flux concentrations are measured in the field. We therefore attempted to derive mass fluxes from resident concentrations by using the temporal moment analysis as described by *Vanderborght and Vereecken* [2001]. The zeroth moment of the travel time is a measure of the tracer mass recovered from the system and the first moment gives the mean travel time.

[17] The first normalized temporal moment $\tau_1(\mathbf{x})$ [T] of a BTC at a node with location $\mathbf{x}$ is defined as

$$\tau_1(\mathbf{x}) = \int_0^\infty t c^f(\mathbf{x}, t) \mathrm{d}t \tag{10}$$

where

$$c^f(\mathbf{x}, t) = \frac{C^f(\mathbf{x}, t)}{\int_0^\infty C^f(\mathbf{x}, t) \mathrm{d}t} = \frac{C^f(\mathbf{x}, t)}{\tau_0(\mathbf{x})} \tag{11}$$

Here, $c^f(\mathbf{x}, t)$ [T^{-1}] is the normalized flux concentration at location $\mathbf{x}$ and time t, and τ_0 [M L^{-3} T] (the zeroth moment) is the area under the BTC measured at location $\mathbf{x}$.

[18] The average solute travel time from the inlet surface to location $\mathbf{x}$, $\mu_t(\mathbf{x})$, is equal to $\tau_1(\mathbf{x})$. The average travel time of an inert solute is used to define the 'equivalent' solute particle velocity $v_{eq}(\mathbf{x})$ [L T^{-1}], which characterizes the BTC measured at location $\mathbf{x}$

$$v_{eq}(\mathbf{x}) = \frac{\Delta x_2}{\mu_t(\mathbf{x})} = \frac{\Delta x_2}{\tau_1(\mathbf{x})} \tag{12}$$

where Δx_2 [L] is the distance between the solute application plane and the monitoring plane. As mentioned above, in practice only resident concentrations are available. We therefore used $c^r(\mathbf{x}, t)$ instead of $c^f(\mathbf{x}, t)$ in equation (11) to arrive at a normalized resident concentration for use in equation (10). This allows us to investigate the suitability and accuracy of this frequently used approximation.

[19] By approximating $v_{2,p,b}$ (the local advection velocity at observation point) in equation (8) by v_{eq} (the average velocity of the particle along its trajectory) for cube p, the solute mass moving in the direction of x_2 can be estimated from the resident concentration at any point using equations (8) and (12).

2.3.3. Leaching Surfaces

[20] For each monitoring plane we prepared leaching surfaces [de Rooij and Stagnitti, 2002a, 2002b, 2004] on the basis of scaled solute mass fluxes

$$m_{p,b}^f = \frac{M_{p,b}^f}{\int_0^{150} \int_5^{15} \int_{25}^{75} M_{p,b}^f \mathrm{d}x_1 \mathrm{d}x_3 \mathrm{d}t} \tag{13}$$

Leaching surfaces leave the original data intact but represent them in a way that facilitates the analysis of the combined variation in space and time of the plotted quantity.

[21] The temporal aspect of solute transport can be expressed in the breakthrough curve (BTC), which describes the travel time distribution [*Jury and Roth*, 1990].

[22] To calculate the leaching surface, the control plane perpendicular to the movement of the solutes needs to be subdivided into small equally sized areas. If we record over time the amount of solute that passed through each area we can construct the BTC for each area. By sorting the areas in descending order of total solute amount passed through each of them we obtain the spatial solute distribution curve (SSDC) [*de Rooij and Stagnitti*, 2000]. A plot of the fraction of the amount of captured solute versus the accumulated area produces the cumulative SSDC.

[23] A leaching surface can be obtained by plotting the individual breakthrough curves (BTCs) of the different areas of the control plane adjacent to one another in order of descending cumulative leaching over the duration of the experiment [*de Rooij and Stagnitti*, 2002a]. By sorting the individual areas, a spatial coordinate y is obtained with dimension L^2. The leaching surface thus has a horizontal time axis and a second horizontal axis (y) that represents the cumulative area of the areas into which the control plane is divided. The vertical axis gives the solute amount, which
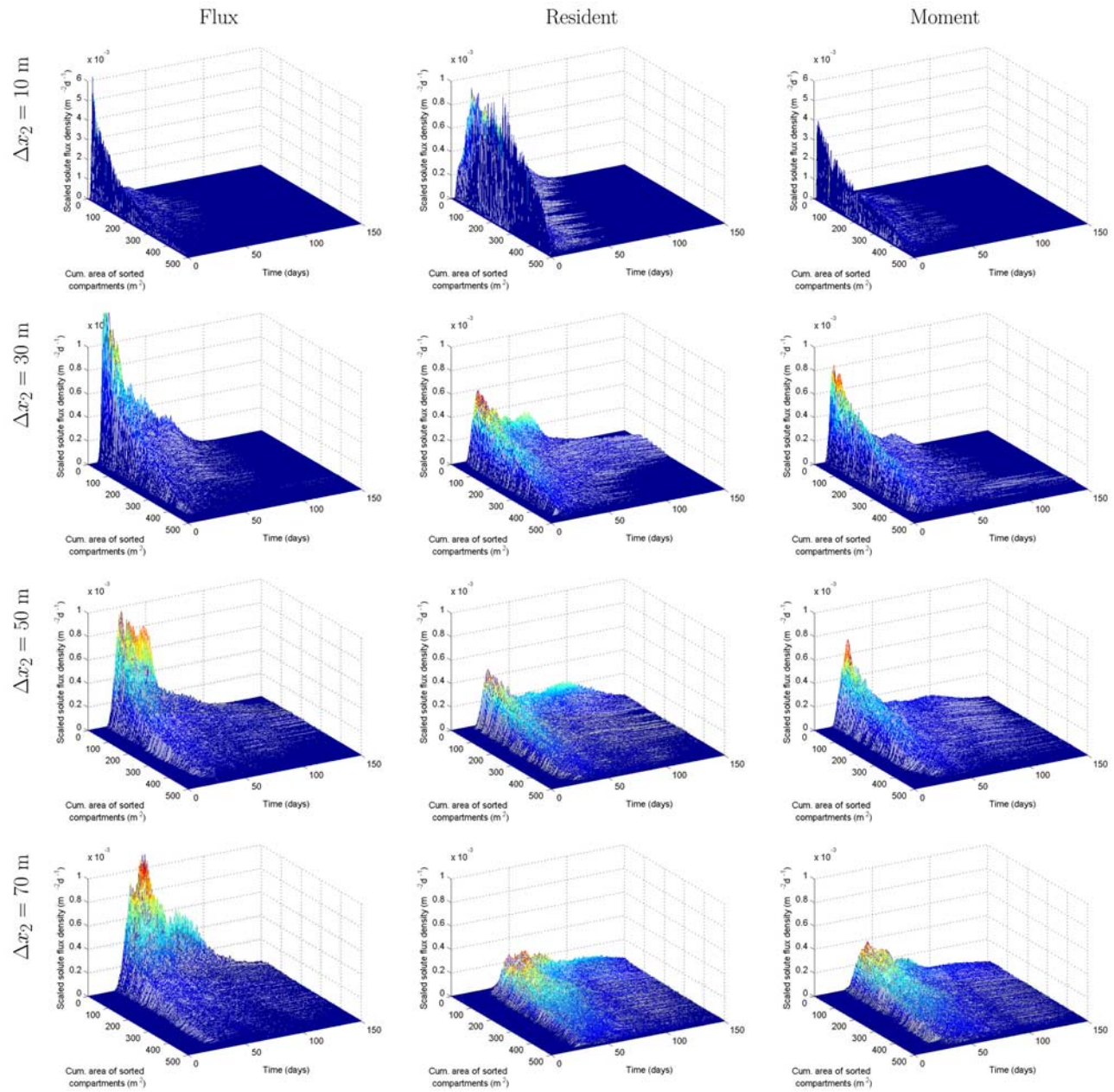
Figure 1. Scaled leaching surfaces of mass fluxes, resident masses, and mass fluxes derived by moment analysis at monitoring planes at the indicated distances from the injection plane. A leaching surface consists of the sorted scaled breakthrough curves (BTCs) in descending order of total solute mass per cell of the analyzed monitoring plane.

Table 1. Maximum Peaks of the Scaled Leaching Surfaces Calculated From Solute Mass Fluxes, Resident Solute Masses, and the Solute Mass Fluxes From the Moment Analysis at Various Distances From the Injection Plane[a]

Downstream Distance From the Injection Plane (m)	Maximum Peak of an Individual Scaled BTC ($m^{-2} d^{-1}$)			Peak of the Overall Scaled BTC ($m^{-2} d^{-1}$)
	Flux	Resident	Moment	
$\Delta x_2 = 10$	6.2×10^{-3}	1.1×10^{-3}	4.0×10^{-3}	1.6×10^{-4}
$\Delta x_2 = 30$	1.6×10^{-3}	6.0×10^{-4}	8.1×10^{-4}	1.0×10^{-4}
$\Delta x_2 = 50$	9.7×10^{-4}	4.8×10^{-4}	7.2×10^{-4}	7.1×10^{-5}
$\Delta x_2 = 70$	1.1×10^{-3}	3.0×10^{-4}	3.8×10^{-4}	5.5×10^{-5}

[a]These are the maximum peaks of individual breakthrough curves (BTCs), which are not necessarily from the first BTC in the scaled leaching surfaces. The last column gives the peak of the BTC for each entire monitoring plane, calculated from the mass fluxes.

can be scaled according to equation (13) to make the leaching surface integrate to unity.

[24] Let $S(y,t)$ [$L^{-2} T^{-1}$] be the resulting leaching surface: the scaled leached amount of solute per area per time. For any location y^*, the solute BTC at that location is the cross section of S parallel to the t axis at y^*:

$$\text{BTC}(t)|_{y^*} = S(y^*, t), \qquad t \in [t_0, \infty) \qquad (14)$$

The cross section parallel to the y axis at time t^* represents the spatial solute distribution curve (SSDC)

$$\text{SSDC}(y)|_{t^*} = S(y, t^*), \qquad x \in [0, A] \qquad (15)$$

where A [L^2] is the combined area of all sampling compartments.

[25] Suitable cross sections of the leaching surface parallel to the time axis or the spatial axis, or integrations along intervals of the space and the time coordinate, can yield a wealth of information about the distribution in space and time of solute movement. For instance, the integral of S over time $\int_0^\infty S(y, t)\,dt$ gives the cumulative SSDC, and the integral over space $\int_0^A S(y, t)\,dy$ gives the BTC of the entire monitoring plane.

[26] For a given flow field, the amount of solute passing a given area depends in a straightforward way on M^f. The relationship between passing amount of solutes and M^r is less unambiguous. The formal definition of the scaled resident mass is

$$\mu_{p,b}^r = \frac{M_{p,b}^r}{\int_0^{20} \int_0^{100} \int_0^{100} M_{p,b}^r \, dx_1 \, dx_2 \, dx_3} \qquad (16)$$

where the denominator is equal to the total injected mass for an inert solute that has not moved out of the flow domain. In our case, strict application of this definition would lead to leaching surfaces that do not integrate to unity, especially far away from the injection plane. We therefore replaced the total injected mass by the mass that resided in a particular monitoring plane during the simulation period. Similar to equation (13) we approximate $\mu_{p,b}^r$ by $m_{p,b}^r$ according to

$$m_{p,b}^r = \frac{M_{p,b}^r}{\int_0^{150} \int_5^{15} \int_{25}^{75} M_{p,b}^r \, dx_1 \, dx_3 \, dt} \qquad (17)$$

We computed pseudoleaching surfaces for the monitoring planes on the basis of the $m_{p,b}^r$ and compared them to the leaching surfaces based on the scaled solute mass fluxes. Finally we constructed leaching surfaces on the basis of approximate scaled solute mass fluxes derived from the temporal moment analysis. Thus, the results of the various analyses are presented consistently, facilitating comparison.

[27] In order to show the impact of high spatial resolution measurements, we also constructed the overall averaged BTCs for each monitoring plane. This is the BTC that

Table 2. Maximum Fraction of the Captured Solute Mass Flowing Through an Individual Cell at Various Distances From the Injection Plane[a]

Downstream Distance From the Injection Plane (m)	Largest Amount of Solute Passing Through an Individual Cell[b]		
	Flux	Resident	Moment
$\Delta x_2 = 10$	3.0×10^{-2}	1.1×10^{-2}	6.4×10^{-3}
$\Delta x_2 = 30$	2.1×10^{-2}	1.0×10^{-2}	7.6×10^{-3}
$\Delta x_2 = 50$	1.9×10^{-2}	1.2×10^{-2}	8.3×10^{-3}
$\Delta x_2 = 70$	2.7×10^{-2}	7.2×10^{-3}	5.8×10^{-3}

[a]The maximum fraction is calculated from solute mass fluxes, resident solute masses, or moment analysis. This maximum fraction is the total amount of solute of the first BTCs in the scaled leaching surfaces.
[b]Fraction of total mass captured at the monitoring plane.

would be obtained by adding the solute fluxes of all grid cells in a monitoring plane and dividing by the monitoring plane area.

3. Results and Discussion

3.1. Mass Fluxes From the Model Output

[28] Figure 1 presents the leaching surfaces at the monitoring planes, each constructed of 10000 individual BTCs. Moving downstream from the injection, the peaks descend (mainly between $\Delta x_2 = 10$ and 30 m) (Figure 1 and Table 1). The maximum amount of solute passing through a single compartment changes only slightly (Table 2). Individual BTCs thus flatten and widen with increasing travel distance (Figure 2). The overall averaged BTCs (for the entire monitoring plane) (Figure 3) also flatten and widen with increasing travel distance.

[29] At all distances a limited fraction of the cross section carries most of the solutes: 25% of the solutes is displaced by 4.5 to 5.9% of the cells for the different monitoring planes (Table 3 and Figure 4). The BTCs of these compartments vary considerably within one leaching surface (Figure 5). This may reflect the limited role of dispersion in high-velocity flow tubes versus a larger effect of dispersion in low-velocity stream tubes.

[30] Despite the fact that transport occurs by an imposed convective-dispersive transport regime at the local scale, solute transport at the aquifer scale is dominated by a few stream tubes in the total pore volume, as indicated by the fact the 50% of the solute transport occurs through less than 16.7% of the cross section anywhere in all four monitoring planes (Table 3).

[31] The leaching surfaces indicate that 75% of the solute mass passed a vertical cross section through only 35% of its area. However, this does not imply that the fraction of the pore volume in which solutes are transported is only 35% of the total pore volume. If this were so, then the peak of the average solute fluxes should arrive already after 0.35 pore volumes, which was not the case. This indicates that the parts of the cross sectional area where most of the solute mass breakthrough occurs are not perfectly connected with areas of high solute flux in all other cross sectional areas. The lack of connection follows from the structure of the heterogeneity that we considered; that is, Gaussian random fields in which high-conductivity zones are not necessarily connected to each other. The poor connectivity of high-flow regions implies that each flow tube can have a wide range of flow velocities along its trajectory and the average velocity
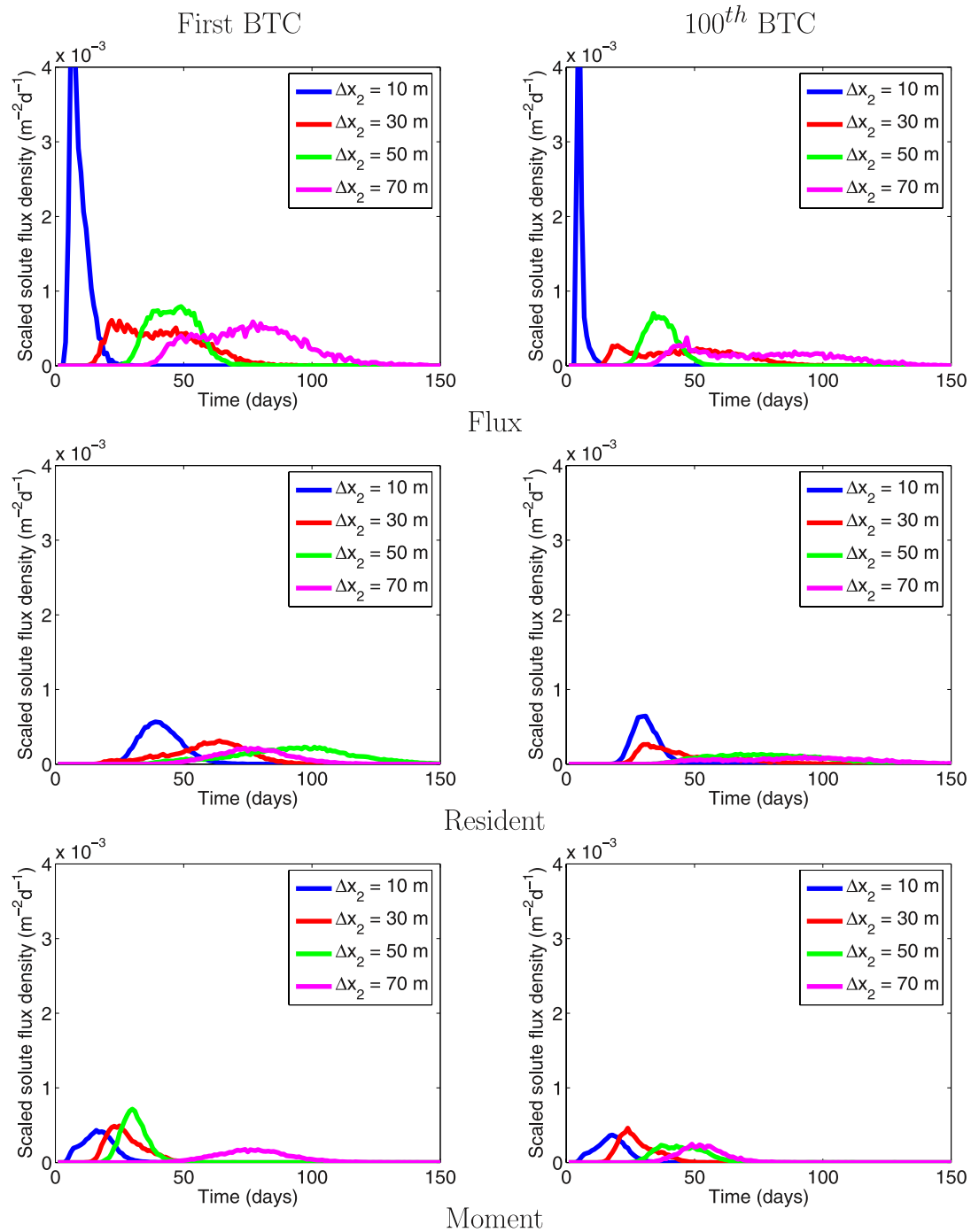
Figure 2. Breakthrough curves for the monitoring planes at the indicated distances (Δx_2) from the injection plane. The BTCs were obtained from mass fluxes, resident masses, and mass fluxes through moment analysis. The BTCs were determined for individual grid cell walls between four nodes. The first and hundredth BTC are shown, as determined by the area under the curve. (The peak of the first flux BTC at $\Delta x_2 = 10$ m is 4.8×10^{-3} (m^{-2} d^{-1}), and the peak of the hundredth flux BTC at $\Delta x_2 = 10$ m is 5.4×10^{-3} (m^{-2} d^{-1})).

will vary among stream tubes, but will always be lower than the peak velocity. The variation in travel times expressed in the leaching surfaces, and the variation of flow velocities between and within stream tubes are consequential if kinetic processes (e.g., sorption) are important along the solute particle trajectories, for example with reactive barriers.

[32] Figure 6 presents the actual amount of cells carrying solute per time step. From Figures 3 and 6 it is evident that high-flow cells carry most of the solute: the scaled solute flux density peaks are well ahead of the maximum cross-sectional extent of the solute plume for $\Delta x_2 = 30$ and 50 m. Also, the maximum percentage of active cells in Figure 6 are consistently lower than the percentage of cells that carried most of the solute mass at some time during the simulated period (Table 3). This indicates that not all cells carried solutes at the same time, even when the bulk of the solutes passed a monitoring plane.
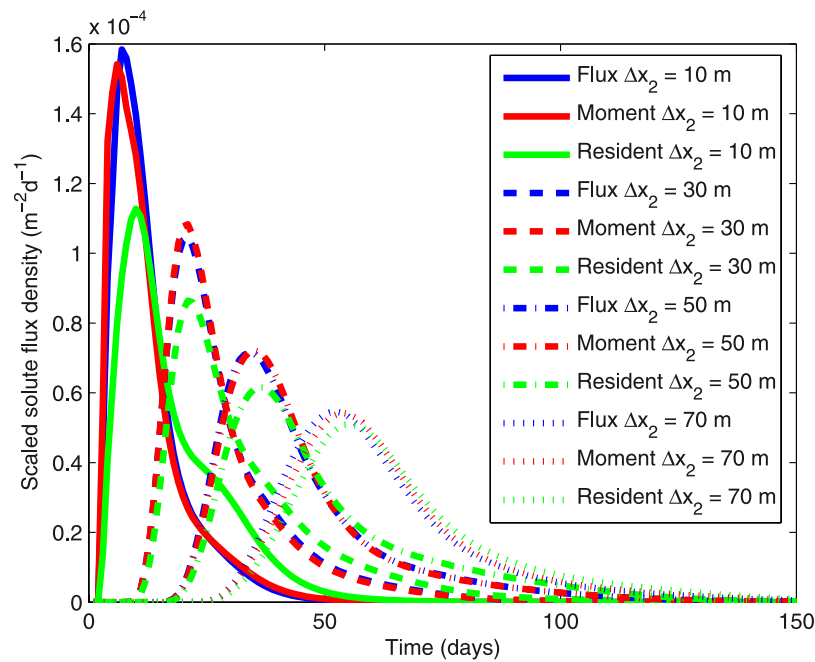
Figure 3. BTCs at the scale of the monitoring planes at the indicated downstream distances from the injection plane. The solute flux densities were derived from solute mass fluxes or resident solute mass or through moment analysis.

[33] The injected mass at the injection surface is equal in each cell. After a short distance this mass is already redistributed toward zones with a higher water flux (Figure 1). The crests of the leaching surfaces are similar to the observed trends in v_2 (Figure 7). This also shows the importance of the velocity field.

[34] Because the overall BTC is an average over the entire control area, the peak height of 1.6×10^{-4} m^{-2} d^{-1} is significantly lower than the maximum peak height of a single cell in the same area (Table 1). With the increase in spatial resolution it becomes obvious that overall BTCs underestimate the local concentration. A regulatory concentration limit can still be exceeded as the maximum peaks are not known with overall BTCs.

3.2. Resident Mass Compared to Mass Fluxes

[35] According to Table 3, slightly more cells contained mass (resident mass) than transported mass (mass fluxes) throughout the aquifer, indicating a small fraction of solute particles that hardly moved. Given the fact that these particles were not only found near the injection plane, they were not permanently stagnant, possibly owing to the random dispersive movement.

[36] The effect of the inappropriate use of resident mass for solute transport is very detrimental to the leaching surfaces (Figure 1), which become erratic and irregular. The noisy appearance of these pseudoleaching surfaces reflects the random (dispersive) process that causes particles to arrive in low-flow regions of the aquifer. The difference between the leaching surfaces based on mass fluxes and resident masses is entirely caused by the different weighting factors assigned to the resident concentrations (equations (7) and (8)). The conversion factor is given by equation (9), and in that equation, only $v_{2,p,b}$ varies between the cells that contributed to the leaching surface. The difference between

the leaching surfaces in the left and middle plots of Figure 1 suggests that dispersion was important in delivering solutes at various locations, but that the velocity field had a massive impact on the movement of these solutes.

[37] The maximum solute flux density peak for the resident mass leaching surfaces is an order of magnitude too low (Table 1 and Figure 2) and occurs much too late, because the resident mass underrepresents rapidly moving solutes in small portions of the flow domain. This leads to slightly delayed overall averaged BTCs with underestimated peaks (Figure 3). The SSDCs for the resident mass (Figure 4) underestimate the importance of the cells through which most of the solute passed. This effect is least pronounced at

Table 3. Percentage of Cells Responsible for Different Fractions of Displaced Solute Mass at the Monitoring Planes[a]

Downstream Distance From the Injection Plane (m)	Fraction of Total Displaced Mass Captured	Percentage of Cells		
		Flux	Resident	Moment
$\Delta x_2 = 10$	0.25	5.3	7.7	11.9
	0.50	16.4	19.9	28.7
	0.75	35.9	40.7	51.7
	1.00	98.1	98.2	92.1
$\Delta x_2 = 30$	0.25	5.3	9.3	10.5
	0.50	15.0	23.6	25.4
	0.75	32.0	44.7	46.3
	1.00	98.5	98.7	90.2
$\Delta x_2 = 50$	0.25	5.9	9.1	11.6
	0.50	16.7	24.0	27.0
	0.75	35.6	46.3	47.7
	1.00	99.8	99.8	93.7
$\Delta x_2 = 70$	0.25	4.5	11.0	12.5
	0.50	15.7	27.4	29.2
	0.75	36.8	50.7	52.2
	1.00	99.2	99.4	97.0

[a]The cells are sorted in descending order of cumulative transferred solute mass.
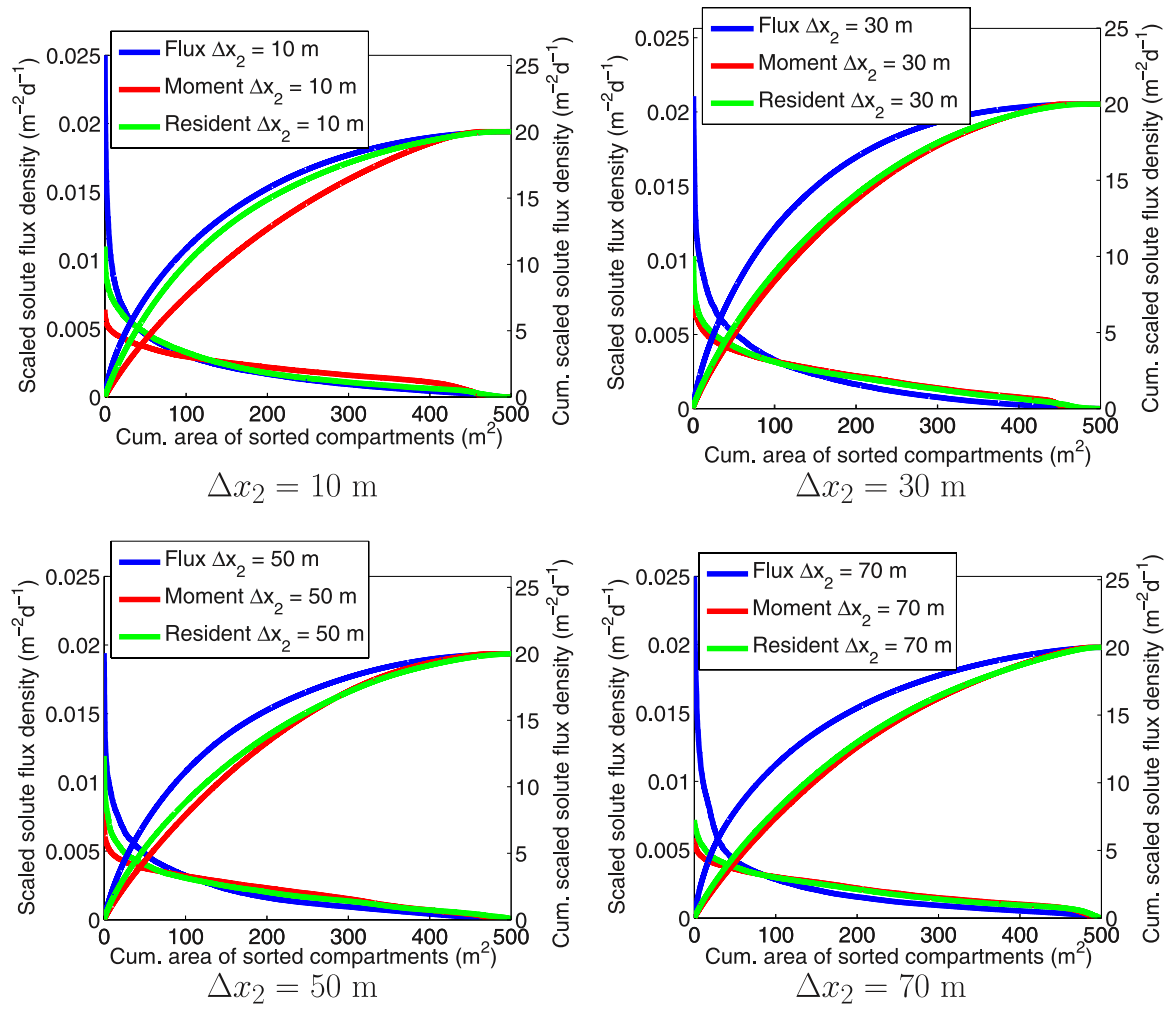
Figure 4. The spatial solute distribution curves (SSDCs) and the cumulative SSDC for the monitoring planes.

10 m after the injection plane. This reflects the nature of the solute application in this study, which imposed a uniform resident concentration. In conclusion, the value of resident solute masses in describing solute movement hinges critically on the degree of detail and accuracy of the available information about the velocity field. For field studies, this poses a formidable observational challenge.
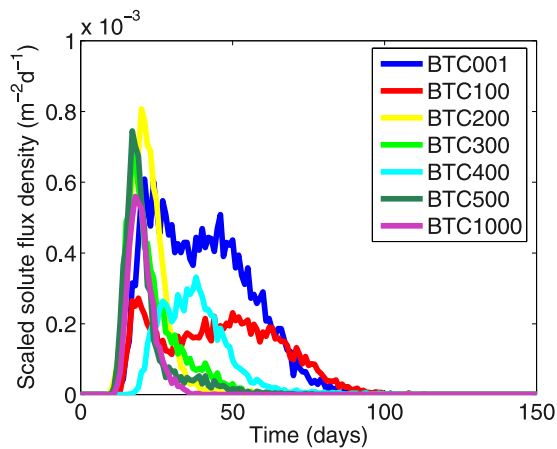
Figure 5. Individual BTCs of monitoring plane $\Delta x_2 = 30$ m based on mass fluxes. These BTCs show the differences of shape of the BTCs within a monitoring plane. The numbers in the legend indicate the rank number based on the area under the curve.
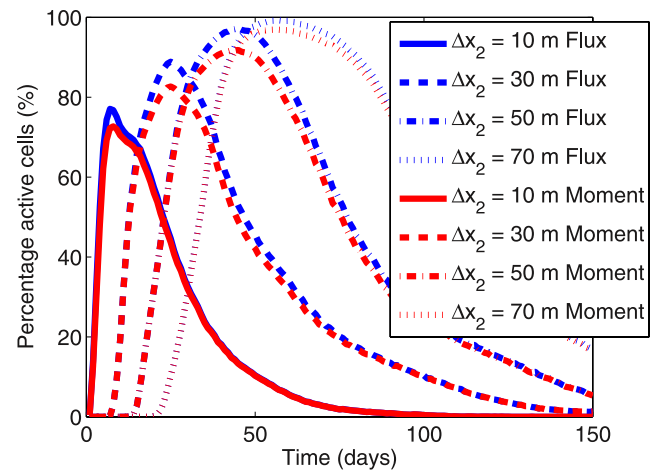

Figure 6. Number of active cells (cells containing solute particles) per time step based on flux masses and on estimated flux masses at the indicated monitoring planes.
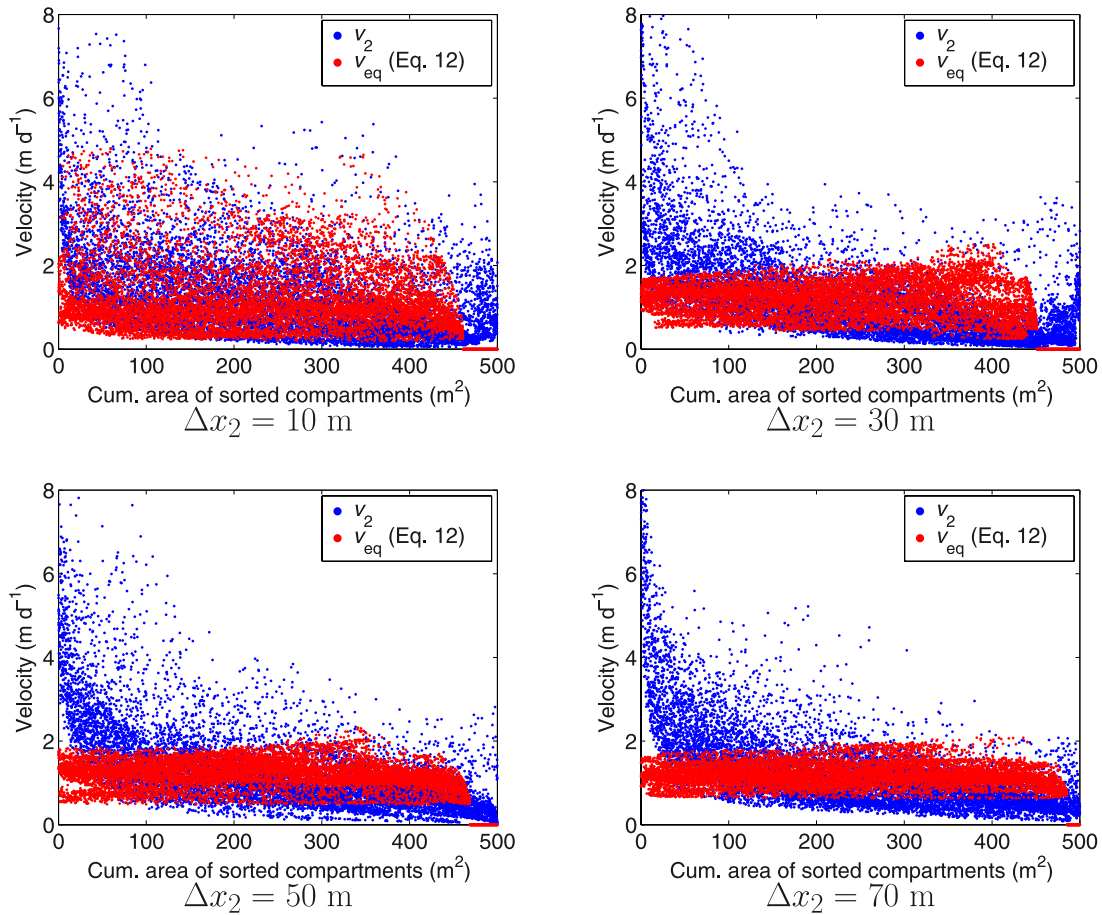
Figure 7. The pore water velocities in the main flow direction (x_2), v_2, of the individual cells in the monitoring planes at the indicated distance downstream of the solute injection plane. The cells are sorted in descending order of the total amount of solute that passed through them. In addition to the true water velocity, the trajectory-averaged pore water velocity (v_{eq}) according to equation (12) is also given.

[38] The coefficient of variation between the peak heights of the individual BTCs from which the leaching surfaces are constructed are between 113 and 130% for the mass fluxes and between 55 and 65% for the resident masses for the various monitoring planes. The difference stems from the additional variation of $v_{2,p,b}$ that adds to the variation of $C^r_{p,b}$ in equation (8) as compared to equation (7).

3.3. Measured and Estimated Mass Fluxes Compared

[39] Estimating the conversion factor in equation (8) by using $v_{eq}(x)$, from equation (12), to approximate $v_{2,p,b}$ significantly improves the leaching surfaces (Figure 1) and the overall averaged BTCs (Figure 3) compared to the use of resident masses for solute transport problems. The effect on local BTCs (Figure 2) and the SSDCs (Figure 4) is considerably smaller. Temporal moment analysis improved the estimation of the time to peak (Figures 2 and 3), while the amount of solutes passing a plane is still underestimated (Figures 2 and 4). The degree of convergence of solute transport toward a limited portion of the cross section is underestimated because of the averaging of the flow velocity over the trajectory (Tables 2 and 3 and Figure 7). The approximate pore water velocities are significantly lower than the real ones for the high-flow cells, but higher for the low-flow cells (Figure 7). The maximum peak at the monitoring planes of individual BTCs is consistently lower than those derived from the mass fluxes (Table 1). These findings corroborate the importance of the pore water velocity field evidenced by the poor results obtained when using only resident solute mass.

[40] To save computation time, we imposed a minimum number of particles present in a cube to produce nonzero concentration, this resulted in a noncontinuous flow velocity distribution (Figure 7) as calculated from the temporal moments. The effects of this manifest themselves in the crest of the leaching surfaces, at the sharp levelling of the SSDCs (Figure 4), at the number of cells carrying solutes (Figure 6 and Table 3), and by the number of cells with subthreshold concentrations (Figure 1).

[41] The distribution of solute passage over the cells varies little with travel distance (Table 3). The use of resident concentrations in the moment analysis consistently leads to overestimation of the percentage of cells carrying a given fraction of the solute, particularly for the cells in the first quantile.

4. Conclusions

[42] The leaching surfaces we constructed highlighted the dominating role of the spatial pore water velocity field. Lateral dispersion had very little effect on the spatiotemporal distribution of solutes at any cross section perpendicular to the macroscopic flow direction. This illustrates the importance of the velocity field, even if dispersion is significant.

[43] This study shows that assessing solute movement from resident concentrations should be done with care. Only if the local concentrations vary weakly within the pore space, resident concentrations give reliable results. This implies that diffusion and dispersion must have had sufficient time to reduce local concentration gradients. This numerical study shows that for a realistic degree of heterogeneity, travel distances of 70 m are still insufficient to acquire the necessary degree of local mixing. In the range where resident and flux concentrations have not yet converged, moment analysis can help improve the results obtained from resident concentration observations.

[44] Moment analysis performed adequately for evaluating solute movement over the entire cross sections of the aquifer. Its approximation of the local velocity by averaging over the trajectory affected its performance at the scale of individual grid cells. Leaching surfaces proved to be an adequate tool to demonstrate, illustrate, and quantify the limitations of moment analysis.

[45] It is likely that the difference between resident and flux masses increases with increasing aquifer heterogeneity and with increasing connectivity of conductive areas. The degree of heterogeneity in our study was by no means extreme. For aquifers with more pronounced variation and/or high-flow regions, the conclusions above become even more pertinent. It is desirable to develop methodologies to measure flux concentrations or solute mass fluxes.

[46] This paper introduced the leaching surface methodology to groundwater hydrology, and applied it to demonstrate the risks involved with misinterpreting resident concentrations. Many other issues remain. The methodology could be applied to other geometries, for instance by creating curved monitoring planes around wells along isochrones

Appendix A: Flux and Resident Concentrations

[47] In a soil with water and solutes moving through the pore space we can define a water content field, a concentration field (both scalar fields), and a flux density field (vector field):

$$\theta(x_1, x_2, x_3, t) \qquad C(x_1, x_2, x_3, t) \qquad q_1(x_1, x_2, x_3, t)$$
$$q_2(x_1, x_2, x_3, t) \qquad q_3(x_1, x_2, x_3, t) \tag{A1}$$

where θ denotes the volumetric water content, C [M L^{-3}] the point solute concentration, q_a [L T^{-1}] the flux density in principal direction a, x_a [L] the spatial coordinate in principal direction a, and t [T] time. In defining C as a point concentration, we imply that the scale of analysis is well beyond the molecular scale. For scales approaching the pore scale, the water content field becomes an indicator field that takes the value of 1 wherever liquid water is present, and equals 0 in the solid and gas phases. The other fields are only defined where the indicator field equals 1, and the flux density field is identical to the flow velocity field. For the scale of the representative elementary volume (REV), q represents the Darcian flux density, and θ is continuous but can have a (spatially variable) residual value below which flow cannot occur. All components of the flux density field are zero if θ is at its residual value.

[48] Note that, even at this scale, q and θ are considered heterogeneous within the REV. Therefore, hydrodynamic dispersion is assumed to be captured by the variation of the flux density field and does not need to be described by a dispersion tensor. Molecular diffusion is the only spreading mechanism not accounted for the flux density field, and is neglected here.

[49] The resident concentration within a given (incremental) soil volume can be calculated by weighting the concentrations in that volume by the volumes of water having these concentrations:

$$C^r(x_1, x_2, x_3, t) = \lim_{\Delta x_1^* \downarrow 0 \Delta x_2^* \downarrow 0 \Delta x_3^* \downarrow 0} \frac{\displaystyle\int_{x_1 - \frac{1}{2}\Delta x_1^*}^{x_1 + \frac{1}{2}\Delta x_1^*} \int_{x_2 - \frac{1}{2}\Delta x_2^*}^{x_2 + \frac{1}{2}\Delta x_2^*} \int_{x_3 - \frac{1}{2}\Delta x_3^*}^{x_3 + \frac{1}{2}\Delta x_3^*} \theta(\xi_1, \xi_2, \xi_3, t) C(\xi_1, \xi_2, \xi_3, t)\, d\xi_3 d\xi_2 d\xi_1}{\displaystyle\int_{x_1 - \frac{1}{2}\Delta x_1^*}^{x_1 + \frac{1}{2}\Delta x_1^*} \int_{x_2 - \frac{1}{2}\Delta x_2^*}^{x_2 + \frac{1}{2}\Delta x_2^*} \int_{x_3 - \frac{1}{2}\Delta x_3^*}^{x_3 + \frac{1}{2}\Delta x_3^*} \theta(\xi_1, \xi_2, \xi_3, t)\, d\xi_3 d\xi_2 d\xi_1} \tag{A2}$$

corresponding to selected travel times to the well. In such studies it should be possible to vary the number of sampling locations and the sampling frequency to optimize measurement strategies in view of acceptable risks and required costs. Applications to other aquifers with different geometries, heterogeneity structures, flow rates, and source configurations is desirable to assess the importance of these aspects for the behavior of contaminants. We demonstrated the potential of leaching surfaces to analyze subsurface solute movement and hope it will see more widespread applications.

where the superscript r denotes a resident concentration, and ξ_a [L] is an integration variable in direction a. The superscript * serves to distinguish the grid-scale length intervals from the larger-scale travel distances elsewhere in the paper. Analogously, we define the flux concentration at an incremental area of a plane defined by a constant value of one of the principal components (we choose x_2 here) during an incremental time interval as the amount of solute passing through the area during the time interval divided by the volume of water passing through:

$$C^f(x_1, x_3, t, x_2) = \lim_{\Delta x_1^* \downarrow 0 \Delta x_3^* \downarrow 0 \Delta t \downarrow 0} \frac{\displaystyle\int_{x_1 - \frac{1}{2}\Delta x_1^*}^{x_1 + \frac{1}{2}\Delta x_1^*} \int_{x_3 - \frac{1}{2}\Delta x_3^*}^{x_3 + \frac{1}{2}\Delta x_3^*} \int_{t - \frac{1}{2}\Delta t}^{t + \frac{1}{2}\Delta t} q_2(\xi_1, \xi_3, \chi, x_2) C(\xi_1, \xi_3, \chi, x_2) d\chi d\xi_3 d\xi_1}{\displaystyle\int_{x_1 - \frac{1}{2}\Delta x_1^*}^{x_1 + \frac{1}{2}\Delta x_1^*} \int_{x_3 - \frac{1}{2}\Delta x_3^*}^{x_3 + \frac{1}{2}\Delta x_3^*} \int_{t - \frac{1}{2}\Delta t}^{t + \frac{1}{2}\Delta t} q_2(\xi_1, \xi_3, \chi, x_2) d\chi d\xi_3 d\xi_1} \tag{A3}$$

where the superscript f denotes a flux concentration, and χ [T] is an integration variable. In the definition of flux concentrations in equation (A3), we neglected the solute flux due to local-scale dispersion so that the local resident and flux concentrations are assumed to be equal, which follows from equations (A2) and (A3) when the integrating interval goes to 0. This assumption implies that the local dispersive flux, which depends on the local-scale dispersion coefficient, can be neglected compared with the advective flux. This condition is fulfilled when the local-scale Peclet number, which is a measure for the ratio of the advective to dispersive fluxes and is defined as $\Delta x_2 / \lambda_L$ (with Δx_2 the lateral travel distance), is sufficiently large.

[50] Both equations are valid for the pore, REV, and macroscopic scales, provided that the θ field is treated as an indicator field at the pore scale, as discussed above.

[51] In the limit as the integration intervals go to zero, both equations refer to the same parcel of water centered around (x_1, x_2, x_3) at time t, and the resident and flux concentrations become identical. However, for nonzero integration intervals, as will occur with every sensor and every sampling protocol, the volume of water residing in the vicinity of (x_1, x_2, x_3) at time t will be different from the volume passing through a plane around (x_1, x_2, x_3) during a time interval centered at t, and the values of C^r and C^f will diverge. The most obvious case is that of a small fraction of highly mobile water and a large fraction of immobile water with a nonuniform concentration in the water phase. The resident concentration is dominated by the immobile water, because it contributes heavily to the integration over the water content field in equation (A2), while the small fraction of mobile water contributes only little. In contrast, the immobile water has no effect whatsoever on the flux concentration because its q_a is zero.

References

Adams, E. E., and L. W. Gelhar (1992), Field study of dispersion in a heterogeneous aquifer: 2. Spatial moments analysis, *Water Resour. Res.*, 28, 3293–3307.

Anderson, M. P. (1987), Field studies in groundwater hydrology: A new era, *Rev. Geophys.*, 25, 141–147.

Aris, R. (1956), On the dispersion of a solute in a fluid flowing through a tube, *Proc. R. Soc. London, Ser. A*, 235, 67–78.

Bear, J. (1972), *Dynamics of Fluid in Porous Media*, Elsevier, New York.

Bellin, A., and Y. Rubin (2004), On the use of peak concentration arrival times for the inference of hydrogeological parameters, *Water Resour. Res.*, 40, W07401, doi:10.1029/2003WR002179.

Boggs, J. M., S. C. Young, L. M. Beard, L. W. Gelhar, K. R. Rehfeldt, and E. E. Adams (1992), Field study of dispersion in a heterogeneous aquifer: 1. Overview and site description, *Water Resour. Res.*, 28, 3281–3291.

Bolt, G. H. (1982), Movement of solutes in soil: Principles of adsorption/exchange chromatography, in *Soil Chemistry: B. Physio-chemical Models*, *Dev. Soil Sci.*, vol. 5, edited by G. H. Bolt, pp. 285–348, Elsevier, Amsterdam.

Dagan, G., V. Cvetkovic, and A. Shapiro (1992), A solute flux approach to transport in heterogeneous formations: 1. The general framework, *Water Resour. Res.*, 28, 1369–1376.

Dagan, G., P. Indelman, and G. Moltyaner (1997), Stochastic analysis of concentration measurements in the transport experiment at Twin Lake site, *Water Resour. Res.*, 33, 559–567.

de Rooij, G. H., and F. Stagnitti (2000), Spatial variability of solute leaching: Experimental validation of a quantitative parameterization, *Soil Sci. Soc. Am. J.*, 64, 499–504.

de Rooij, G. H., and F. Stagnitti (2002a), Spatial and temporal distribution of solute leaching in heterogeneous soils: Analysis and application to multisampler lysimeter data, *J. Contam. Hydrol.*, 54, 329–346.

de Rooij, G. H., and F. Stagnitti (2002b), The solute leaching surface as a tool to assess the performance of multidimensional unsaturated solute transport models, in *Pre-conference Proceedings of the International Conference on Computational Methods in Water Resources, Delft, the Netherlands*, edited by S. M. Hassanizadeh et al., pp. 639–646, Elsevier, Amsterdam.

de Rooij, G. H., and F. Stagnitti (2004), Applications of the beta distribution in soil science, in *Handbook of Beta Distribution and Its Applications*, edited by A. K. Gupta, and S. Nadarajah, pp. 535–550, Marcel Dekker, New York.

Freyberg, D. L. (1986), A natural gradient experiment on solute transport in a sand aquifer: 2. Spatial moments and the advection and dispersion of nonreactive tracers, *Water Resour. Res.*, 22, 2031–2046.

Garabedian, S. P., D. R. LeBlanc, L. W. Gelhar, and M. A. Celia (1991), Large-scale natural gradient tracer test in sand and gravel, Cape Cod, Massachusetts: 2. Analysis of spatial moments for a nonreactive tracer, *Water Resour. Res.*, 27, 911–924.

Gelhar, L. W., C. Welty, and K. R. Rehfeldt (1992), A critical review of data on field-scale dispersion in aquifers, *Water Resour. Res.*, 28, 1955–1974.

Hess, K. M., S. H. Wolf, and M. A. Celia (1992), Large-scale natural gradient tracer test in sand and gravel, Cape Cod, Massachusetts: 3. Hydraulic conductivity variability and calculated macrodispersivities, *Water Resour. Res.*, 28, 2011–2027.

Jury, W. A., and K. Roth (1990), *Transfer Functions and Solute Movement Through Soil*, 226 pp., Birkhauser, Basel, Germany.

Jury, W. A., and D. R. Scotter (1994), A unified approach to stochastic-convective transport problems, *Soil Sci. Soc. Am. J.*, 58, 1327–1336.

Killey, R. W. D., and G. L. Moltyaner (1988), Twin Lake tracer tests: Setting, methodology, and hydraulic conductivity distribution, *Water Resour. Res.*, 24, 1585–1612.

Kraichnan, R. H. (1970), Diffusion by a random velocity field, *Phys. Fluids*, 13, 22–31.

Kreft, A., and A. Zuber (1978), On the physical meaning of the dispersion equation and its solutions for different initial and boundary conditions, *Chem. Eng. Sci.*, 33, 1471–1480.

LeBlanc, D. R., S. P. Garabedian, K. M. Hess, L. W. Gelhar, R. D. Quadri, K. G. Stollenwerk, and W. W. Wood (1991), Large-scale natural gradient tracer test in sand and gravel, Cape Cod, Massachusetts: 1. Experimental design and observed tracer movement, *Water Resour. Res.*, 27, 895–910.

Mackay, D. M., D. L. Freyberg, P. V. Roberts, and J. A. Cherry (1986), A natural gradient experiment on solute transport in a sand aquifer: 1. Approach and overview of plume movement, *Water Resour. Res.*, 22, 2017–2029.

Moltyaner, G. L., and R. W. D. Killey (1988), Twin Lake tracer tests: Longitudinal dispersion, *Water Resour. Res.*, 24, 1613–1627.

Neuendorf, O. (1997), Numerische 3D-simulation des Stofftransports in einem heterogenen Aquifer, technical report, Forschungszent. Juelich, Juelich, Germany.

Parker, J. C., and M. T. van Genuchten (1984), Flux-averaged and volume-averaged concentrations in continuum approaches to solute transport, *Water Resour. Res.*, 20, 866–872.

Ptak, T., and G. Schmid (1996), Dual-tracer transport experiments in a physically and chemically heterogeneous porous aquifer: Effective transport parameters and spatial variability, *J. Hydrol.*, 183, 117–138.

Ptak, T., and G. Teutsch (1994), Forced and natural gradient tracer tests in a highly heterogeneous aquifer: Instrumentation and measurements, *J. Hydrol.*, 159, 79–104.

Rehfeldt, K. R., J. M. Boggs, and L. W. Gelhar (1992), Field study of dispersion in a heterogeneous aquifer: 3. Geostatistical analysis of hydraulic conductivity, *Water Resour. Res.*, 28, 3309–3324.

Rubin, Y., and S. Ezzedine (1997), The travel times of solutes at the Cape Cod tracer experiment: Data analysis, modeling, and structural parameters inference, *Water Resour. Res.*, 33, 1537–1547.

Sudicky, E. A. (1986), A natural gradient experiment on solute transport in a sand aquifer: Spatial variability of hydraulic conductivity and its role in the dispersion process, *Water Resour. Res.*, 22, 2069–2082.

Sudicky, E. A., J. A. Cherry, and E. O. Frind (1983), Migration of contaminants in groundwater at a landfill: A case study. 4. A natural-gradient dispersion test, *J. Hydrol.*, 63, 81–108.

Vanderborght, J., and H. Vereecken (2001), Analyses of locally measured bromide breakthrough curves from a natural gradient tracer experiment at Krauthausen, *J. Contam. Hydrol.*, 48, 23–43.

Vanderborght, J., A. Kemna, H. Hardelauf, and H. Vereecken (2005), Potential of electrical resistivity tomography to infer aquifer transport char-

acteristics from tracer studies: A synthetic case study, *Water Resour. Res.*, *41*, W06013, doi:10.1029/2004WR003774.

Vereecken, H., G. Lindenmayr, O. Neuendorf, U. Döring, and R. Seidemann (1994), TRACE, a mathematical model for reactive transport in 3D variable saturated porous media, *ICG-4 Internal Rep. 501494*, Forschungszent. Juelich, Juelich, Germany.

Vereecken, H., U. Döring, H. Hardelauf, U. Jaekel, U. Hashagen, O. Neuendorf, H. Schwarze, and R. Seidemann (2000), Analysis of solute transport in a heterogeneous aquifer: The Krauthausen field experiment, *J. Contam. Hydrol.*, *45*, 329–358.

Woodbury, A. D., and Y. Rubin (2000), A full-Bayesian approach to parameter inference from tracer travel time moments and investigation of scale effects at the Cape Cod experimental site, *Water Resour. Res.*, *36*, 159–171.

_____

E. Bloem, Bioforsk, Norwegian Institute for Agricultural and Environmental Research, Frederik A. Dahls vei 20, N-1432 Ås, Norway. (esther.bloem@bioforsk.no)

G. H. de Rooij, Soil Physics, Ecohydrology and Groundwater Management, Environmental Sciences Group, Wageningen University, P. O. Box 47, NL-6700 AA Wageningen, Netherlands.

J. Vanderborght, Agrosphere, ICG-4, Forschungszentrum Jülich, D-52425 Jülich, Germany.